International Journal of Thermophysics, Vol. 23, No. 5, September 2002 (© 2002)

On the Critical Point of Tungsten[1]

A. D. Rakhel,[2,3] A. Kloss,[4,5] and H. Hess[4]

Experimental results of exploding tungsten wire experiments with heating rates of 10^{10} to 10^{11} $K \cdot s^{-1}$ are interpreted using a one-dimensional hydrodynamic model. The vaporization dynamics under these conditions are discussed. It is shown that for the wires used the superheating of the liquid phase is small and vaporization starts close to the binodal line of the phase diagram. Due to inertia, a volume vaporization takes place in a thin surface layer, while in the bulk of the column formed by the exploding wire a pressure of the order of 10 kbar is maintained. Sufficiently uniform density and temperature distributions are formed in the liquid core surrounded by the two-phase layer. This behavior of vaporizing wires was used to obtain the thermal expansion coefficient of liquid tungsten along with its critical point parameters.

KEY WORDS: critical point; evaporation; exploding wires; numerical modeling; superheating; thermal expansion; tungsten.

1. INTRODUCTION

A theoretical description of liquid metal thermodynamics is a very complex problem, which is still far from a solution. Thermodynamic properties have been investigated experimentally mainly for alkali metals and mercury up to their critical points. Critical point parameters of refractory metals have been estimated using corresponding states or semiempirical rules [1]. Such estimations usually give large scatter in the critical constants, and their accuracy is very uncertain. For example, estimates for the critical temperature of tungsten are in the range of 12,000 to 23,000 K and the critical

[1] Paper presented at the Sixth International Workshop on Subsecond Thermophysics, September 26–28, 2001, Leoben, Austria.

[2] Institute for High Energy Densities, Izhorskaya 13/19, Moscow 127412, Russia.

[3] To whom correspondence should be addressed. E-mail: savlab@iht.mpei.ac.ru

[4] Institute of Low-Temperature Plasma Physics, University of Greifswald, Friedrich-Ludwig-Jahn-Str. 19, D-17489 Greifswald, Germany.

[5] Present address: OSRAM GmbH, Hellabrunner Str. 1, D-81536 München, Germany.

0195-928X/02/0900-1369/0 © 2002 Plenum Publishing Corporation

pressure is between 3 and 16 kbar. Several dynamic techniques were applied to determine the critical parameters experimentally. Martynyuk and Karimkhodzhaev [2] have proposed to use exploding wires for this purpose. In Refs. 3 and 4 this approach was developed using more extensive diagnostics. Due to lack of information about the exploding wire dynamics, the experimental results were interpreted using some assumptions. In particular, the vaporization was assumed to start at a spinodal.

In the present paper results obtained in exploding wire experiments are interpreted using a one-dimensional numerical model describing the hydrodynamic flow and the vaporization dynamics. The work is both theoretical and experimental. Experiments on exploding tungsten wires with heating rates of 10^{10} to 10^{11} $K \cdot s^{-1}$ have been performed. The model describes adequately the exploding wire dynamics over the entire range of heating rates. It is shown that for tungsten wires used in these experiments (wires manufactured without any purification procedure to remove the nucleation centers), the superheating of the liquid phase is small and the vaporization starts close to the binodal. Due to inertia, the volume vaporization takes place in a surface layer while a high level of pressure is maintained in the bulk of the column formed by the exploding wire. Sufficiently uniform density and temperature distributions are maintained in the liquid core surrounded by the two-phase layer. The thermodynamic state of the layer is strongly inhomogeneous. The model shows that at heating rates of the order of 10^{11} $K \cdot s^{-1}$ the thickness of the layer remains small compared to the liquid core radius during a sufficiently long period of time. This behavior of vaporizing wires was used to investigate thermophysical properties of tungsten at substantially higher temperatures and pressures than those attained in slower experiments [5–7].

2. EXPERIMENTS

Two series of experiments were carried out in air at atmospheric pressure with tungsten wires having a diameter of 75 μm and a length of 5 mm. The wires (supplied by Goodfellow Metals) were of 99.99% purity by weight as reported by the manufacturer. In the first series heating was accomplished by discharging a capacitor of 327 nF charged to an initial voltage of 2.2 to 4.6 kV through the wire; in the second series the capacitor had a value of 675 nF and its initial voltage was in the range 3.8 to 6.6 kV. The discharge circuit used provides an electrical current with a density of $(3 \text{ to } 7) \times 10^7$ $A \cdot cm^{-2}$ in the wire. Under these conditions the Joule heat dissipated in the wire reaches the cohesive energy after 100 to 500 ns depending on the initial voltage. A coating (polytetrafluorethylene) with a thickness of 14 μm was used to avoid a peripheral gas-discharge.

The diagnostics used in these experiments are described in Refs. 8 and 9. The voltage across the wire was measured by means of an ohmic divider and the current through it by a Rogowski coil. The current and voltage are measured with a precision of 0.5%. The current signals of different experiments with all parameters constant show a scatter of less than 2%. The voltage signal scatter is about 3%. The temperature was deduced from the radiance of the column surface measured at a wavelength of 650 nm (with an uncertainty of less than 8%). The diameter of the expanding column was determined from a streak camera image caused by self-luminosity with a precision of 3% and a scatter of 7%. Shadowgraphs obtained using a Xe flashlight were used to observe the column at low temperatures ($T < 7{,}000$ K). Four images of the entire column with an exposure time of 10 ns each for pre-chosen instants were obtained with a fast framing camera. These images are used to ensure that the symmetry of the column does not change, and that gas-discharges do not develop in the surrounding air. From this set of measured quantities, the specific enthalpy, temperature, density, electrical conductivity, and their mutual dependencies are obtained. More than 20 experiments for each series were performed. Only one parameter was varied within a series: the initial voltage. Every experiment was repeated three times to get the information about the reproducibility and uncertainty for the measured quantities.

3. HYDRODYNAMIC MODEL

A one-dimensional model was developed to describe the hydrodynamic flow in a metal undergoing thermal expansion and vaporization when an electrical current pulse is applied [9, 10]. The set of equations consists of the local laws of conservation of mass, linear momentum, and energy together with Maxwell's equations. A one-dimensional magnetohydrodynamic flow with Z-pinch symmetry is considered. In a cylindrical coordinate system the z-axis is directed along the axis of the wire, and all physical quantities are functions of the radius vector r and the time t only. The only nonzero component of velocity is the radial component u, the electrical current density has only the component along the z-axis j, and the magnetic field strength has only the azimuthal component H. The laws of conservation can be written as

$$\frac{\partial \rho}{\partial t} + \frac{1}{r}\frac{\partial}{\partial r}(r\rho u) = 0 \tag{1}$$

$$\frac{\partial (\rho u)}{\partial t} + \frac{1}{r}\frac{\partial}{\partial r}(r\rho u^2) = -\frac{\partial p}{\partial r} - \frac{1}{c} jH \tag{2}$$

$$\frac{\partial}{\partial t}\left(\rho\varepsilon + \frac{\rho u^2}{2}\right) + \frac{1}{r}\frac{\partial}{\partial r}\left[r\rho u\left(w + \frac{u^2}{2}\right)\right] = jE' \tag{3}$$

where ρ, p, and ε are the density, pressure, and specific inner energy, respectively, $w = \varepsilon + p/\rho$ is the specific enthalpy, and E' is the electrical field strength in the reference frame which is at rest in relation to a particle in the flow. According to the Lorentz formula, $E' = E + uH/c$, where E is the electrical field strength in the laboratory frame of reference, and c is the speed of light in vacuum (the Gaussian system is used). The effects of heat conduction, viscosity, and radiation are negligible, and therefore the corresponding terms were dropped in the dynamical equations, Eqs. (1)–(3). The evaporation from the metal surface can be neglected also, as this process is limited by heat conduction from the bulk to the surface layer.

Maxwell's equations take the form:

$$\frac{\partial E}{\partial r} = \frac{1}{c}\frac{\partial H}{\partial t}; \qquad \frac{\partial H}{\partial r} = \frac{4\pi}{c} j \tag{4}$$

The electrical current density obeys Ohm's law: $j = \sigma E'$ (σ is the electrical conductivity).

The hydrodynamic flow was computed for three regions: tungsten wire, coating, and surrounding air. We assumed that the substances do not mix with each other at their boundaries. The Godunov method [11] was used to solve the dynamical equations, Eqs. (1)–(3). Maxwell's equations were solved by the tridiagonal inversion method described in Ref. 12. The mesh used in these computations consisted of 10 to 50 cells in the wire, 10 to 40 cells in the coating, and 500 to 1000 cells in the surrounding air. Thermodynamic functions of tungsten in the region of the liquid-vapour phase transition were obtained using the equation of state model from Ref. 13.

An equation to represent the electrical conductivity of tungsten as a function of temperature and density was developed for the region of interest according to Ref. 10. For the liquid phase the following function was used:

$$\sigma = \frac{\sigma_{\mathrm{m}} f(\rho)}{1 + \beta_l (T - T_{\mathrm{m}})}; \qquad f(\rho) = 1 + \gamma (1 - \rho/\rho_{\mathrm{m}})^k \tag{6}$$

where T is the temperature, and the subscript m refers to the melting point, i.e., T_{m} is the melting point temperature, σ_{m} is the conductivity of liquid tungsten at the melting point, and ρ_{m} is its density at this point. The constants β_{l}, γ, and k were adjusted using our experimental data. In the supercritical region an interpolation was used, which gives as an asymptote the liquid phase dependence, is smoothly merged at low densities with an ideal plasma dependence, and describes the metal-nonmetal transition in

the intermediate region according to Ref. 14. The ideal plasma conductivity was obtained using Saha's formula to calculate the plasma composition, and taking into account the collisions of electrons with ions and atoms.

It was assumed that in the two-phase liquid-gas region the phases constitute a fine dispersed mixture. The conductivity of the mixture was calculated by means of the effective medium formulae [15]:

$$\sigma = \tfrac{1}{2}(g + \sqrt{g^2 + 2\sigma_1\sigma_2}\,) \tag{7}$$

$$g = [\sigma_1(2-3y) + \sigma_2(3y-1)]/2 \tag{8}$$

where σ_1 is the conductivity of the liquid, σ_2 is the conductivity of the vapor, and y is the volume fraction of the vapor in the mixture. Equations (7) and (8) were applied to describe also the conductivity in the solid-liquid region.

3. ANALYSIS OF VAPORIZATION DYNAMICS

The resistivity without correction for thermal expansion is presented as a function of enthalpy for different heating powers in Fig. 1. The calculated

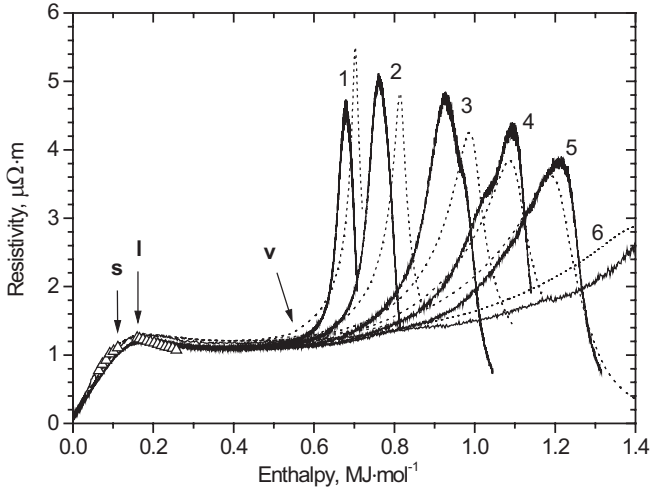

Fig. 1. The resistivity without correction for thermal expansion as a function of enthalpy for six experiments with different heating power: 1, 2.4 TW·mol^{-1}; 2, 3.6 TW·mol^{-1}; 3, 6.3 TW·mol^{-1}; 4, 7.7 TW·mol^{-1}; 5, 8.2 TW·mol^{-1}; 6, 8.8 TW·mol^{-1}. Solid lines, experiments; dotted lines, model. The beginning of melting (**s**), the end of melting (**l**), and the beginning of vaporization (**v**) are designated. Triangles, [6].

dependences were obtained assuming that the vaporization starts at the binodal and the two-phase liquid-vapor mixture is in local thermodynamic equilibrium. At point **v** the resistivity rises because the volume vaporization starts. The volume fraction of the vapor increases and therefore, the well conducting cross-section of the column is reduced because the conductivity of the vapor is substantially lower than that of the liquid metal. The peak in the resistivity is formed when the percolation threshold is achieved for the liquid-gas mixture. The threshold value of y derived from Eqs. (10) and (11) is equal to $2/3$. At the threshold the fine dispersed mixture transforms from the liquid with vapor bubbles distributed in it into the vapor with separated droplets. For $y > 2/3$ the density dependence of the conductivity of the mixture becomes a rather weak function. Therefore, the resistance decreases as the cross-section of the column increases. As can be seen, for the highest heating rate experiments 5 and 6 the resistance of a melted wire is almost constant over a wide range of enthalpy. For experiment 6 a constant value is maintained up to an enthalpy even larger than the cohesive energy of tungsten ($0.848\ \mathrm{MJ \cdot mol^{-1}}$, [16]).

In Fig. 2 the measured and calculated densities are presented as a function of enthalpy. The higher the heating rate, the larger the densities

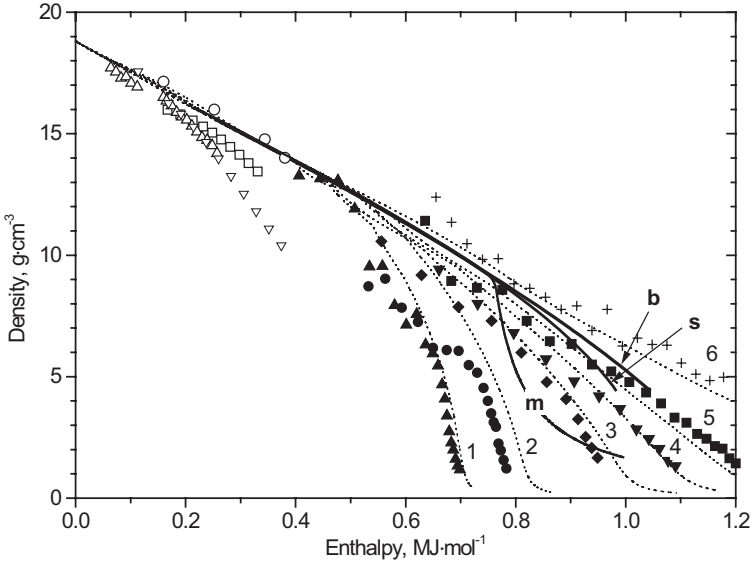

Fig. 2. Density as a function of enthalpy for 6 experiments with different heating powers (see Fig. 1). Solid marks and crosses, experiments; dotted lines, model. Open marks: triangles down, [3]; triangles up, [6]; squares, [7]; circles, [5]. Thick lines: **b**, equilibrium line; **s**, isobar $P = 5$ kbar for superheated liquid; **m**, isobar $P = 5$ kbar for two-phase mixture in thermodynamic equilibrium.

that are reached at a certain value of enthalpy. This behavior is directly related to the volume vaporization dynamics. Qualitative estimates explain this behavior. The sound speed for the liquid-vapor mixture is much lower than that for the liquid phase. For an infinitesimal mass fraction of vapor, the sound speed c_m in such a mixture is

$$c_m = E_{coh} P_s(T)/(R_g T \rho \sqrt{c_p T}) \tag{9}$$

where E_{coh} is the cohesive energy, $P_s(T)$ is the saturation vapor pressure, R_g is the gas constant, c_p is the heat capacity of the liquid, and ρ is its density [17]. At the normal boiling point we obtain $c_m \sim 10^{-3}$ km·s^{-1}, which is much smaller than the speed of sound for liquid tungsten of ~ 3.2 km·s^{-1} [6]. This relation between the sound speeds remains valid at higher temperatures. For example, at $T = 12{,}000$ K, we obtain $c_m \sim 0.1$ km·s^{-1}. Thus, the inertia effects in the two-phase mixture are much stronger as in the liquid and, therefore, the two-phase layer expands relatively slow. This causes a delay in the expansion of the layer, and the delay is larger the higher the heating rate is.

The computation results show that the boiling curve of tungsten must be somewhere close to the data of experiments 5 and 6 (see Fig. 2). If the curve were closer to the data of Refs. 3, 6, and 7, it would not be possible to reach the densities of experiments 5 and 6 since a pressure of the order of 100 kbar would be needed; but the characteristic pressure for experiments 5 and 6 is of the order of 10 kbar. A value of $(4.0 \text{ to } 4.5) \times 10^{-5}$ K^{-1} was obtained for the thermal expansion coefficient of liquid tungsten, which is substantially lower than 8.6×10^{-5} K^{-1} [6] (we used $c_p = 56$ J·mol^{-1}K^{-1} [7]). The data of Lebedev and Savvatimski [5] obtained for wires confined in thick capillaries are in good agreement with our results.

This value of the thermal expansion coefficient along with the literature data for the specific heat capacity, cohesion energy, liquid tungsten melting point density, and the normal boiling point temperature were used to fit the parameters of the equation of state. The fitting procedure is discussed in Ref. 13. As a result we have found: $m = 1$, $n = 9$, $Q = 1.3$, and $c_v = 3.0$. It should be noted that in the equation of state used the specific heat capacity of the ideal gas term (c_v) was also adjusted (in Ref. 13, $c_v = 3/2$). The two remaining fitting parameters can be obtained from the critical point parameters presented below. The experimental dependences for the resistance and the thermal expansion coefficient of liquid tungsten determined were used to fit the parameters in Eq. (6): $\beta_l \approx 2 \cdot 10^{-5}$ K^{-1}, $\gamma \approx 1.0$, and $k \approx 1.4$.

The dependences shown in Fig. 2 were analyzed to estimate the superheating of liquid tungsten in these experiments. It seems to be lower

than the experimental uncertainty. To explain this observation, the isobar $P=5$ kbar corresponding to an overheated liquid (up to a spinodal) is presented. The isobar for the two-phase liquid-vapor mixture in thermodynamic equilibrium is also shown. These isobars and the other thermodynamic functions presented were obtained by means of the equation of state with the set of the fitting parameters as above. If appreciable superheating took place, the curves for experiments 3, 4, 5, and 6 would be located in the narrow region between the binodal (**b**) and the isobar for the superheated liquid (**s**). This is because the characteristic pressure for these experiments was larger than 5 kbar. Figure 2 demonstrates a large difference between the experimental dependences in the region of the liquid vapor phase transition. Therefore we conclude there was no remarkable superheating. Thus the vaporization starts close to the binodal.

The kinetics of volume vaporization for liquid metals is discussed in Ref. 18. A relaxation time for this phase transition in metallic samples made of a fine dispersed powder was estimated to be of the order of 1 ns. This gives superheating of the liquid phase of the order of 100 K for a heating rate of 10^{11} K·s^{-1}. Hence, the two-phase mixture in our experiments can be considered to be almost in local thermodynamic equilibrium. The radiographs presented in Ref. 19 confirm this conclusion showing the bubbles and droplets developed for about 500 ns in tungsten resistively heated to a temperature of 7,000 to 9,000 K.

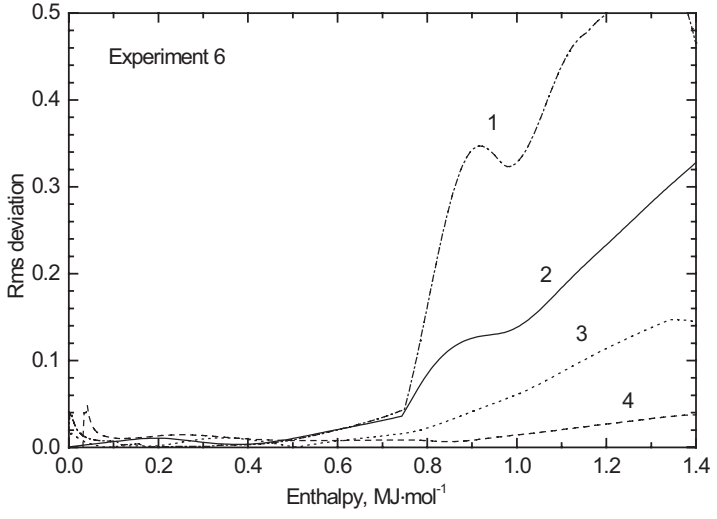

Fig. 3. Root-mean-square (rms) deviations of different measured quantities from their mean values across the column: resistivity (1), density (2), temperature (3), and enthalpy (4).

To better understand the distributions of the measured quantities across the column formed by an exploding wire, in Fig. 3 the root-mean-square (rms) deviations of some quantities from their mean values are depicted. The measured quantities are distributed almost uniform up to an enthalpy of 0.73 $MJ \cdot mol^{-1}$ which is substantially higher than that attained in slower experiments (0.26 to 0.33 $MJ \cdot mol^{-1}$ [5–7]).

4. DETERMINATION OF THE CRITICAL POINT PARAMETERS

The equation of state model can be used to calculate the critical point parameters. The parameters obtained in this way were considered as a first step approximation. In this section we discuss some direct experimental measurements concerning the critical point.

The computation results show that for the experiments with the highest heating rate the inner part of the column passes into the supercritical region of the phase diagram, i.e., supercritical temperatures and pressures are achieved. The first sign of this transition into the supercritical region is the straight-line dependence of the density versus enthalpy occurring for experiments 5 and 6, since such behavior resembles the supercritical isobars having no bents in the liquid-vapor phase transition region. The dependences for the resistance in Fig. 1 confirm this conclusion, showing an almost constant value in this region. Our computations give for experiment 3 a characteristic pressure of 5 to 7 kbar (in an enthalpy range of 0.8 to 0.9 $MJ \cdot mol^{-1}$), for experiment 4 it is 9 to 13 kbar, and for experiment 5 it is 12 to 15 kbar. The slope of the dependency for experiment 5 remains close to that of the boiling curve (**b**) and there are no bents in the liquid-vapor phase transition region, i.e., for the enthalpy $W \leqslant E_{coh}$. The data for experiment 4 deviate remarkably from the boiling curve in this enthalpy range. This means that the two-phase layer becomes rather thick for this experiment. Therefore, the characteristic pressure does not exceed the critical pressure. As a result one may conclude that the critical pressure is somewhere between 9 to 13 kbar.

The second sign that the supercritical region is reached can be recognised in the temperature dependences. Figure 4 depicts the temperature versus enthalpy measured and computed. The five dotted curves are related to five Lagrangian particles, i.e., thin radial layers in the column, representing five zones from 50 zones of the mesh used in these computations. These five curves correspond to the zone at the axis of the wire, the zone at the surface, and three other zones in between. The computed dependences nearly coincide up to an enthalpy of 0.6 $MJ \cdot mol^{-1}$ at which the volume vaporization starts in the surface layer. The temperature in the

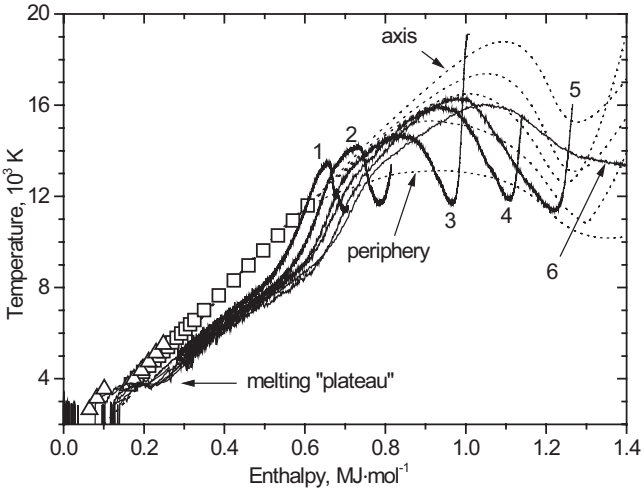

Fig. 4. The measured temperatures (solid lines, numbering see Fig. 1) and calculated temperatures for different radial zones for experiment 5 (dotted lines). Triangles, [6]; squares, [7].

liquid core remains homogeneous up to 0.8 MJ·mol^{-1}. At an enthalpy of 1.0 to 1.1 MJ·mol^{-1} the temperatures reach maxima which is a result of the sharp rise in the resistance (see Fig. 1) causing a decrease in the heating power. The thermodynamic work of the core acting on the surface layer and the coating starts and the pressure begins to decrease. This leads to a temperature decrease after the maximum is reached. At a certain instant the particles leave the two-phase region and the temperatures start to increase again as the specific heat capacity of the gas is substantially lower than that of the two-phase mixture.

Estimations show that the plasma in the surface layer is transparent enough and therefore, the liquid core can be seen through the two-phase layer when the volume fraction of the liquid phase in the layer becomes lower than the percolation threshold. The ionization degree of the plasma at 12,000 to 14,000 K along the coexistence line is 0.03 to 0.05, which gives an absorption length of the order of 10 μm (at 650 nm); the absorption length in the liquid metal is of the order of 0.01 μm. Hence, the temperature at the maximum which can be measured in this case is just the critical temperature. Two facts confirm this conclusion. The temperatures at the maxima for experiments 4, 5, and 6 practically coincide whereas for experiments 1, 2, and 3, they are substantially lower. For these experiments the pressure was lower than the critical pressure. As a result the following set

of the critical point parameters was obtained: $T_C = (16{,}000 \pm 1{,}000)$ K, $P_C = (11 \pm 2)$ kbar, and $\rho_C = (4.5 \pm 0.5)$ g·cm^{-3}.

The critical point of tungsten was estimated by Seydel et al. [3] also measuring the temperature at the maximum. The authors attributed this temperature to the temperature at the spinodal corresponding to the applied pressure. The following critical parameters were obtained in Ref. 3: $T_C = 14{,}000$ K and $P_C = 5$ kbar. It is interesting to note that the equation of state used in the present work gives a boiling temperature of 13,600 K at 5 kbar.

5. CONCLUSIONS

Exploding tungsten wire dynamics at heating rates of 10^{10} to 10^{11} K·s^{-1} can be described by a one-dimensional hydrodynamic model. For tungsten wires used in these experiments (wires manufactured without a special purification procedure to remove the nucleation centers), the superheating of the liquid phase is small. For experiments with the highest heating rates, sufficiently uniform density and temperature distributions are maintained in the expanding column formed by an exploding wire. This peculiarity of the hydrodynamic flow has been used to obtain the thermal expansion coefficient of liquid tungsten ($(4.3 \pm 0.3) \times 10^{-5}$ K^{-1}) along with its critical point parameters: $T_C = (16{,}000 \pm 1{,}000)$ K, $P_C = (11 \pm 2)$ kbar, and $\rho_C = (4.5 \pm 0.5)$ g·cm^{-3}.

REFERENCES

1. H. Hess, *Phys. Chem. Liq.* **30**:251 (1995).
2. M. M. Martynyuk and A. D. Karimkhodzhaev, *Russ. J. Phys. Chem.* **48**:722 (1974).
3. U. Seydel, W. Fucke, and H. Wadle, *Die Bestimmung thermophysikalischer Daten flüssiger hochschmelzender Metalle mit schnellen Pulsaufheizexperimenten* (Verlag Dr. Peter Mannhold, Düsseldorf, 1980).
4. K. Boboridis, G. Pottlacher, and H. Jäger, *Int. J. Thermophys.* **20**:1289 (1999).
5. V. Lebedev and A. I. Savvatimski, *Usp. Fiz. Nauk* **144**:215 (1984).
6. R. S. Hixson and M. A. Winkler, *Int. J. Thermophys.* **11**:709 (1990).
7. E. Kaschnitz, G. Pottlacher, and L. Windholz, *High Press. Research* **4**:558 (1990).
8. A. Kloss, T. Motzke, R. Grossjohann, and H. Hess, *Phys. Rev.* E **54**:5851 (1996).
9. A. Kloss, A. D. Rakhel, and H. Hess, *Int. J. Thermophys.* **19**:983 (1998).
10. V. S. Vorob'ev and A. D. Rakhel, *Teplofiz. Vys. Temp.* **28**:18 (1990).
11. K. Godunov, A. V. Zabrodin, M. Ya. Ivanov, A. N. Kraiko, and G. A. Prokopov, *Numerical Solution of Many-Dimensional Gas Dynamic Tasks* (Nauka, Moscow, 1976).
12. A. A. Samarski and Yu. P. Popov, *Difference Methods for Solution of Gas Dynamic Tasks* (Nauka, Moscow, 1980).
13. D. A. Young, *Lawrence Livermore Laboratory Report No. UCRL-52352* (1977).
14. A. A. Likalter, *Usp. Fiz. Nauk.* **170**(3):831 (2000).
15. R. Landauer, *J. Appl. Phys.* **23**:779 (1952).

16. D. R. Lide and H. P. R. Frederikse, eds, *CRC Handbook of Chemistry and Physics* (CRC Press, Boca Raton, Ann Arbor, London, Tokyo, 1993–1994).
17. L. D. Landau and E. M. Lifshitz, *Fluid Mechanics* (Pergamon Press, Oxford, 1992).
18. L. V. Altshuler, A. A. Bakanova, A. V. Bushman, I. P. Dudalapov, and V. N. Zubarev, *Zh. Exsp. Teor. Fiz.* **73**:1866 (1977).
19. S. A. Pikuz, T. A. Shelkovenko, D. B. Sinars, J. B. Greenly, Y. S. Dimant, and D. A. Hammer, *Phys. Rev. Lett.* **83**:4313 (1999).